Improved Selectivity and Cytotoxic Effects of Irinotecan via Liposomal Delivery: a Comparative Study on Hs68 and HeLa Cells

Ana Casadó[a,b,c], Margarita Mora[a], M. Lluïsa Sagristá[a], Santi Rello-Varona[b,d], Pilar Acedo[b,e] Juan Carlos Stockert[b], Magdalena Cañete[b], Angeles Villanueva[b,f]*

[a] Department of Biochemistry and Molecular Biomedicine, Facultat of Biologia, Universitat de Barcelona, Barcelona, Spain.

[b] Departamento de Biología, Facultad de Ciencias, Universidad Autónoma de Madrid, Madrid, Spain.

[c] Communication Department, Hospital Clinic of Barcelona, Barcelona, Spain.

[d] Sarcoma Research Group, Institut d'Investigació Biomèdica de Bellvitge-IDIBELL, L'Hospitalet de Llobregat, Barcelona 08908, Spain

[e] Division of Surgery and Interventional Science, University College London, London, United Kingdom

[f] Instituto Madrileño de Estudios Avanzados en Nanociencia (IMDEA Nanociencia), Madrid, Spain.

Corresponding Author:
Angeles Villanueva
Departamento de Biología, Facultad de Ciencias, Universidad Autónoma de Madrid.
C/ Darwin 2, E-28049 Madrid, Spain.
Fax: +34 91497 8344Tel: +34 91497 8236
E-mail: angeles.villanueva@uam.es

ABSTRACT

Irinotecan (CPT-11) is an effective chemotherapeutic agent widely used to treat different cancers. Otherwise, the liposomal delivery of anti-tumor agents has been shown to be a promising strategy. The aim of this study has been to analyze the effect of liposomal CPT-11 (CPT-11lip) on two human cell lines (Hs68 and HeLa) to establish the suitability of this CPT-11 nanocarrier. We have demonstrated the highest uptake of CPT-11lip in comparison with that of CPT-11sol, in lactate buffer, and that CPT-11lip was internalized in the cells through an endocytic process whereas CPT-11sol does so by passive diffusion. CPT-11lip was not cytotoxic to normal fibroblast Hs68 cells, but induced a massive apoptosis accompanied by cell senescence in HeLa cells. CPT-11lip treatment modified the morphology of HeLa cells, induced different cell cycle alterations and accumulated into lysosomes in both cell lines. In particular, CPT-11lip treatment showed that surviving HeLa cells remained in a state of senescence whereas only a temporal growth arrest was induced in Hs68 cells. Results of RT-PCR indicated that the different responses in Hs68 (survival) and HeLa cells (apoptotic death), seemed to be induced by a p53- and p53- independent mechanism, respectively. An analysis of DNA damage also determined that released CPT-11 from liposomes was able to reach the nucleus and exert a genotoxic effect in both cell lines, which was repaired in Hs68 but not in HeLa cells. All results indicate that phospholipid-cholesterol liposomes possess optimum properties for CPT-11 delivery, being biocompatible and selectively cytotoxic against HeLa tumorigenic cells.

Keywords: Irinotecan, Liposomes, Cytotoxicity, Drug uptake, Apoptosis, Growth arrest, DNA double-strand breaks

1. Introduction

Irinotecan (CPT-11; 7-ethyl-10-[4-(1-piperidino)-1-piperidino]-carbonyloxy-camptothecin) is one of the most widely used camptothecin (CPT) analogues that belongs to a novel class of antineoplastic agents, called topoisomerase I (Topo I) interactive compounds (Chen and Liu, 1994). CPT-11 is enzymatically converted *in vivo* by a carboxylesterase into its most active cytotoxic metabolite SN-38 (7-ethyl-10-hydroxy-camptothecin) (Wu *et al.*, 2002). Both CPT-11 and SN-38 act by binding to Topo I, responsible for the relaxation of supercoiled duplex DNA during replication, inhibiting DNA synthesis (Hsiang *et al.*, 1985; Gracía-Carbonero and Supko, 2002).

CPT-11 has long been applied in the clinical treatment of various types of tumors (Liew and Yang, 2008). The whole of the published results established CPT-11 as one of the most active drugs in the first- and second-line chemotherapeutic treatment against colorectal cancer (CRC) due to its confirmed evidence of anti-tumor efficacy (Vanhoefer *et al.*, 2001). Of special interest was the demonstration of considerable activity of this drug against 5-fluorouracil (5-FU)-refractory colorectal cancer (Díaz-Rubio, 2004). Moreover, camptothecins have also been successfully used to treat other types of cancers (Liu *et al.*, 2016; Iyer *et al.*, 2015).

Nevertheless, camptothecin derivatives show some limitations, the principal related to the coexistence of a chemical equilibrium between an E ring-opened carboxylate form and a lactone form: the former has less than 10% the potency of the lactone form as Topo I inhibitor and it is inactive in cell culture, perhaps due to inability to cross the cell membrane (Teicher, 2008).

The main adverse side effects associated to camptothecins therapies are neutropenia, thrombocytopenia, anemia and a number of non-hematological toxic effects after prolonged administration (Estanqueiro *et al.*, 2015). Numerous studies have reduced the incidence of the common complications of CPT-11 treatment, besides increasing its clinical effectiveness, in terms of overall survival, progressive-free survival and response rates (Hind *et al.*, 2008). In an

attempt to improve first- and second-line chemotherapy regimens, some investigators have combined novel biological agents with CPT-11 or oxaliplatin and 5-FU, whereas others have proposed the use of selective delivery carriers.

Some systemic and targeted therapies have recently been investigated and evaluated in metastatic CRC and the results have been discussed and reviewed by Hedge et al. (2008) and Köhne and Lenz (2009). Targeted agents have expanded the available treatment options for patients with metastaic CRC, prolonging survival when combined with the standard cytotoxic CPT-11-, oxaliplatin- and fluoropyrimidine-based regimens. Despite these gains, the overall impact of current targeted agents in the treatment of mCRC has been relatively modest, and while 2-year survival has improved, no gains have been, as of yet, in 5-years survival (Chu, 2012).

On the other hand, some innovations and developments in nanotechnology have revolutionised cancer therapeutics to solve one of the major drawbacks of cytostatics: most of the current agents do not differentiate cancerous from normal cells, giving systemic toxicity and a series of adverse effects that limit the maximum allowable dose of the drug. Thus, in the last decade, numerous efforts are being made to investigate new drug delivery systems with a double aim: i) to promote tumor drug accumulation, and ii) to reduce doses needed for effective treatment, with the consequent decrease of the side effects (Deshpande *et al.*, 2013). Therefore, one of the main challenges in human disease treatment is no longer the development of more efficient drugs, but the improvement of drug selectivity (Juillerat-Jeanneret and Schmitt, 2007).

In this sense, the use of liposomes has been proposed as a promising nanotherapeutic approach to increase the therapeutic index of a wide range of antineoplastic agents (De Jong and Borm, 2008; Sen and Mandal, 2013; Przybylo *et al.*, 2016). Liposomes have been shown to improve the pharmacokinetics and tumor localization of encapsulated drugs, modify the toxicities associated with a particular drug, and ultimately enhance antitumor efficacy compared with the unencapsulated drug (Drummond *et al.*, 2008). Numerous liposomal formulations bearing

cancer therapeutics have been approved or are currently undergoing clinical trials (Bozzuto and Molinari, 2015). The consideration of the chemical properties of cytostatics is a pivotal aspect to get the appropriate formulation for any drug. Hydrophilic or hydrophobic molecules are differently incorporated into nanotechnological devices and, when considering liposomes, their solubility properties determine the greater or lesser encapsulation efficiency. The study of the molecular interactions between the constituents of the carrier and the drug is also important to predict the extent of drug encapsulation.

In vivo studies have shown that CPT-11 is an ideal candidate for encapsulation in different types of nanocarriers, liposomes included (Messerer *et al.*, 2004; Ramsay *et al.*, 2008). Liposome encapsulation can provide an internal aqueous environment of low pH that stabilizes the active, ring-closed, lactone form of the drug, easily hydrolysable at physiologic pH (Burke and Bom, 2000; Burke and Gao, 1994): the liposomal encapsulation of CPT-11 would thus provide a potent drug formulation for the treatment of different types of cancer. In October 2015, the U.S. Food and Drug Administration approved an encapsulated form of CPT-11 in liposomes (Onivyde, Merrimack Pharmaceuticals, Inc), previously known as MM-398 (Chustecka, 2015), which use in combination with fluorouracil and leucovorin in patients with metastatic pancreatic cancer has been approved in several countries (Lamb and Scott, 2017). This paper presents a study about the suitability of a liposomal formulation of CPT-11 (CPT-11lip) for cancer therapy protocols and a comparative analysis with a healthy and a malignant cell line has been performed to establish the possible specificity of a CPT-11lip-based chemotherapy. Different efficient and sophisticated methodologies, based on active loading procedures, have been reported in the literature to entrap the basic CPT-11 (pKapiperidino = 11.20) into liposomes. While effective in their ability to encapsulate the drug, they have some general disadvantages such as long manufacturing procedures, difficulties in removing some of the materials used to increase the encapsulation rate and high manufacturing costs.

Herein, we are reporting the characteristics and the efficiency of CPT-11 loaded temperature sensitive liposomes. Thermosensitive responsiveness had been incorporated as a criterion for the design of the liposomal formulation of this drug, being this property especially useful to ensure the integrity of the carrier when administered *in vivo*, besides allowing a controlled release of the drug in the therapeutic sites in response to temperature increases (Casadó *et al.*, 2014). The feasibility as delivery vehicles and the potential of this nanomedicine have been determined by evaluating *in vitro* the cellular uptake, cytotoxic behavior and cell death mechanism.

2. Materials and Methods

A more detailed version of the M&Ms employed in this study can be found as Supplementary Material.

2.1. Preparation of liposomal CPT-11

Intermediate unilamellar liposomes (IUVs) were prepared by vortexing and extrusion as previously reported (Casadó et al., 2014). Briefly, lipids, DSPC, DOPS and CHOL (Avanti Polar Lipids, USA), were mixed in a molar ratio of 65:35:30 (Casadó *et al.*, 2016) to prepare the lipid film and CPT-11 was added from a chloroform/methanol (2:1) solution at a 7.5:1 molar ratio. Multilamellar vesicles (MLVs) were prepared by hydrating the dried lipid films in 10 mM lactate buffer (pH 4.4) to a final lipid concentration of 10 mg/mL. MLVs dispersions were frozen (liquid N_2) and thawed (55 °C water bath) above the phase transition temperature (Tm) for five times. For IUVs preparation, MLVs were extruded (Lipex Biomembranes, Canada) six times through 400 nm and twelve times through 200 nm polycarbonate membrane filters (Osmonics, USA). Control liposomes without CPT-11 were also prepared.

The ability of the IUVs to keep encapsulated their cargo was determined by carboxyfluorescein leakage experiments and the liposomes were visualized by transmission electron microscopy

(TEM), characterized by size, polydispersity index and ζ-potential and by quantifying the amount of the drug inside vesicles. Total and entrapped CPT-11 was systematically quantified by absorbance spectroscopy as described previously (Casadó *et al.*, 2014).

2.2. Cell cultures and treatments

Hs68 non-transformed fibroblasts and the tumor epithelial cell line HeLa (cervix adenocarcinoma), were purchased from American Type Culture Collection (USA). Cells were grown in DMEM supplemented with 50 U/mL penicillin, 50 µg streptomycin/mL and 10% FCS. Cells were maintained in a 5% CO_2 atmosphere at 37 °C. Cells were incubated with 100 µM CPT-11 entrapped in liposomes (CPT-11lip) or solubilized in 10 mM lactate buffer pH 4.4 (CPT-11sol), depending on the type of assay, at different times between 0 and 48 h to assess the cellular uptake of the drugs using flow cytometry and at 24 h to visualize subcellular localization by fluorescence microscopy. For cell survival studies, cell cycle analysis and morphological studies, a period of 48 h of incubation with post-incubation times up to 48 h, were used.

2.3. Measurement of CPT-11 uptake and internalization

Cells were treated with CPT-11lip or CPT-11sol up to 48 h. CPT-11 fluorescence was measured with a LSR II flow cytometer (BD Biosciences, USA) using excitation and emission wavelengths of 405 and 450 nm, respectively. Significance was assessed using a Student's paired t-test.

To analyze internalization mechanisms of CPT-11, cells were incubated with 100 µM of CPT-11lip or CPT-11sol for 3 h at 4 °C. Then, samples were washed three times with PBS and directly observed by fluorescence microscopy (under UV excitation) combined with phase contrast microscopy. Moreover, cells incubated for 24 h, were observed by confocal fluorescence microscopy combined with phase contrast microscopy under UV excitation. To analyze the possible participation of lysosomes in drug accumulation, cells were also incubated

with 1 mL DMEM containing 50 nM LysoTracker Red DND-99 (Life Technologies, USA) for 30 min, washed three times with PBS and visualized by confocal microscopy.

2.4. Analysis of cell morphology

Morphological changes at different times (0, 24 and 48 h) after incubation with 100 μM CPT-11lip were assessed by toluidine blue staining using bright field microscopy.

2.5. Cell survival assessment

Thiazolyl blue (MTT; Sigma-Aldrich, USA) reduction and Trypan blue (Sigma-Aldrich) exclusion tests were used for the assessment of cell survival. Production of MTT formazan precipitates, dissolved in 100 μL DMSO per well, was measured as absorbance at 540 nm in a SpectraFluor spectrophotometer (Tecan, Switzerland). Cell survival was expressed as the percentage of absorption of treated cells in comparison with that of control cells. For Trypan blue exclusion test, treated and untreated cells were trypsinized (harvesting also the detached ones) and mixed with the same volume of a 0.2 % Trypan blue solution in PBS. Cell counting of death (blue) or alive (white and bright) cells was performed using a Neubauer hemocytometer (Marienfeld, Germany). Data correspond to mean values ± standard deviation from at least eight different experiments for MTT assay and four different experiments for Trypan blue assay.

2.6. Cell death mechanisms

2.6.1. Necrosis analysis

Induction of necrosis was determined by measuring the activity of the enzyme LDH, released into the culture medium by necrotic cells following lethal membrane injury, by using a fluorimetric assay kit (CytoScan-Fluoro), following the manufacturer's instructions (G-

Biosciences, USA). Fluorescence was measured with an excitation at 560 nm and emission at 590 nm after shaking the plates for 15 s in a SpectraFluor spectrophotometer. The percentage of cytotoxicity was calculated by using the average fluorescence values from experimental, maximum LDH release, and culture medium background.

2.6.2. Apoptosis identification

Apoptotic nuclear morphology of detached HeLa cells after incubation with CPT-11lip was visualized by H-33258 staining as previously described by us (Rello et al., 2005). Apoptosis was confirmed by immunofluorescence staining of pro-apoptotic Bax protein (monoclonal mouse anti-Bax sc-20067; Santa Cruz Biotechnology, USA).

2.7. Cell cycle analysis

Cell cycle phase distribution in both cell lines was analyzed by flow cytometry using Propidium iodide (PI) DNA staining. Measurements were performed with an Epics XL flow cytometer (Beckman Coulter, USA) with an argon laser line at 488 nm and complemented with the appropriate filters. Cell fractions in sub G1, G0/G1, S, G2/M and > 4C phases were quantified in histograms with Summit software. Identification of apoptotic cells (sub G1 region) was achieved by determination of hypoploid cell populations. Polyploid cells were also identified in the > 4C region.

2.8. Senescence-associated β-galactosidase staining

Senescence was assessed by measuring the β-galactosidase activity using the Senescence Cells Histochemical Staining Kit (Sigma-Aldrich). The percentage of senescent cells was calculated by the number of β-galactosidase-positive cells (blue cells) out of at least 500 cells from different microscope fields.

2.9. Quantitative real-time PCR

Cells were treated with CPT-11lip for 3 to 48 h, and the total RNA was extracted. Two μg of total RNA from each sample was used for cDNA synthesis using the SuperScriptTM III First-Strand Synthesis System for RT-PCR according to the manufacturer's instructions (Invitrogen, USA). Quantitative RT-PCR amplifications were performed with TaqMan Gene Expression Assays products in an ABI PRISM 7900 HT Sequence Detection System (Applied Biosystems). The following genes were analyzed: TP53 (Hs00153349_m1), Bax (Hs00180269_m1) and Bcl-2 (Hs00608023_m1). A sample without cDNA was used as negative control and glyceraldehyde-3-phosphate dehydrogenase (GAPDH) (Hs99999905_m1) was used as internal control. The expression level of the target gene in the treated cells was measured relative to the level observed in the untreated cells and was quantified using the formula $2^{-\Delta\Delta CT}$ (Livak and Schmittgen, 2001).

2.10. Cytoskeleton analysis

To get insight into the cytoskeleton disorganization after CPT-11lip treatment, adhesion to substrate was analyzed by fluorescent labelling against the focal contact proteins vinculin (monoclonal anti-vinculin clone hVIN-1, Sigma-Aldrich) and F-actin (phalloidin–tetramethylrhodamine B isothiocyanate, phalloidin-TRITC, Sigma-Aldrich).

2.11. DNA damage response by immunodetection of γ-H2AX

Hs68 and HeLa cells grown on glass coverslips and incubated with CPT-11lip for different times (3, 6 and 24 h) were immunostained for phosphorylated histone H2AX (monoclonal mouse anti-γ-H2AX antibody, Merck Millipore).

2.12. Live cell imaging studies

Untreated control cells as well as cells incubated with CPT-11lip or empty liposomes were visualized at different times under phase contrast inverted microscope.

2.13. Optical microscopy

Observations of samples processed for optical microscopy (bright field and fluorescence) were made with an Olympus BX61 epifluorescence microscope equipped with an Olympus DP50 digital camera (Olympus, USA), and processed using the Photoshop CS5 software (Adobe Systems, USA). In immunofluorescence determinations, cell nuclei were counterstained using H-33258 (5 μg/mL in distilled water, 5 min) and mounted with ProLong Gold antifade reagent (Thermo Fisher Scientific). Confocal microscopy was performed using a multispectral Leica TCS SP5 confocal microscope (Leica, Germany). In addition, time-lapse images of living cells were captured with an inverted microscope Leica DMI 6000B equipped with a Leica DFC420 C digital camera (Leica) and images were processed with the same software.

3. Results and Discussion

3.1. Characterization of CPT-11 loaded liposomes

Different methodologies have been reported in the literature to entrap CPT-11 into liposomes. All of these are based in active loading strategies: gradient loading-stabilization techniques, based in the formation of intraliposomal drug-polyanion complexes; other transmembrane gradient methods using ammonium sulfate, pH changes with or without the incorporation of ionophres and divalent cations to the liposome bilayers; or formulations with phosphorylated carbohydrates such as phytic acid (Ramsay *et al.*, 2008; Hattori *et al.*, 2009; Neijzen *et al.*, 2015).

Besides the method, to procure optimal drug formulations and efficient drug delivery systems it is essential to control the physicochemical parameters of the vehicle (Peetla *et al.*, 2009). By using different biophysical techniques we carried out a study of the molecular interactions between the constituents of the carrier and the drug and established the suitability of a ternary lipid mixture for encapsulating CPT-11 with high efficacy. We demonstrated that CPT-11, positively charged in its piperidine group at acidic pH, interacts electrostatically with the DOPS component of the DSPC/DOPS/CHOL bilayer, making stable the incorporation of a high percentage of the drug into liposomes (Casadó *et al.*, 2016).

We have considered the different formulation strategies (passive or active drug loading) and the different options to enhance drug delivery reported in the literature *(Oliveira Eloy et al., 2014; Pattni et al., 2015).* Finally, we choose passive drug loading and triggered delivery approaches to formulate CPT-11 in liposomes and developed an easy-to-perform, high-efficciency encapsulation method to prepare liposomes loaded with CPT-11(Casadó *et al.*, 2014). Thus, the designed liposomes were endowed with the ability to control the release of the drug by means of responsiveness to temperature. The synthesis protocol was standardized and the liposomal suspension, procured from the DSPC/DOPS/CHOL (65:35:30) lipid mixture and a lipid/drug molar ratio of 7.5:1, was systematically and rigorously characterized by size, polydispersity index (0.114 ± 0.032) and ζ-potential and by quantifying the amount of the drug inside vesicles. In this regard, drug encapsulation efficiency (DEE% = 85.3 ± 6.2) and drug loading efficiency (DLE% = 11.8 ± 0.9) were calculated as the amount of drug inside liposomes with respect to the total amount of drug or lipids added in preparing formulation, respectively. The 5(6)-carboxyfluorescein aqueous marker was used to determine *in vitro* the drug retention ability and the trapped volume of the formulated liposomes. A new kinetic analysis of the CF release curves was carried out by fitting the data to an exponential curve by means the non-lineal regression program Graph Pad Prism (version 5.00) and the percent

leakages at the equilibrium (Feq) have been evaluated at different temperatures and in the absence and in the presence of serum. All the characterization parameters corresponding to the budgets used in the experiments given in this paper are listed in Table 1 and are in good agreement with our previous published data (Casadó *et al.*, 2014). TEM images showed the round shape of CPT-11lip (see Fig. S1B).On the other hand, the permeability analysis shows the effect of temperature on the CF release rate and that the efflux of CF increased in the presence of serum. Furthermore, at physiological temperature, the very small values of Feq highlight the high stability of the designed liposomal formulation.

Table 1. Physicochemical (A) and permeability (B) parameters of DSPC/OOPS/CHOL (65:35:30) liposomes

A Sample Composition	[a]Vesicle size (nm)	[b]ζ-Potential (mV)	[c][CPT-11] (mM)	mg CPT-11/ mmol phospholipid
DSPC/OOPS/CHOL 65:35:30	148.3 ± 8.5	- 42.5 ± 2.7	----	----
DSPC/OOPS/CHOL/CPT-11 65:35:30:17.3	157.0 ± 12.9	- 49.1 ± 4.8	[d]1.74 ± 0.12	107.7 ± 0.0

B [d]Trapped Volume	F_{eq} (%)								
	37 °C			41 °C			45 °C		
µLCF/µmol lipid	0	25	250	0	25	250	0	25	250
1.6 ± 0.1	2.6 ± 0.4	12.6 ± 0.2	18.1 ± 1.9	5.7 ± 0.4	26.9 ± 3.5	32.2 ± 3.3	4.6 ± 0.9	10.8 ± 1.2	10.9 ± 1.5

[a] Particle size measured as Z average mean.

[b] ζ-potential determined by laser-Doppler anemometry.

[c] Bulk encapsulated drug concentration in the liposomes suspension (for CPT-11 loaded liposomes)

[d] Determined by carboxyfluorescein dye retention (for empty liposomes)

3.2. Efficient cellular uptake of CPT-11lip by endocytosis

Uptake and accumulation of CPT-11 incorporated into liposomes (CPT-11lip) and dissolved in lactate buffer solution (CPT-11sol) into Hs68 and HeLa cells, was determined by flow cytometry measuring the intrinsic fluorescence properties of this camptothecin derivative under ultraviolet excitation. As shown in Fig 1A, the amount of CPT-11 inside cells increases as a function of incubation time and in both cell lines was greater for CPT-11lip than CPT-11sol. Likewise, uptake kinetics depends on cell line, being the uptake at initial time faster and higher for normal fibroblast Hs68 cells. Taken together, these studies indicated that CPT-11 in this liposomal formulation was capable of an extensive cellular internalization into both cell lines. Previously, we had shown that CPT-11lip displayed greater drug uptake compared with the non-liposomal CPT-11 formulation in human colon carcinoma Caco-2 cells (Casadó *et al.*, 2014).

Internalization mechanism of CPT-11lip and CPT-11sol inside both cell types was analyzed after 3 h of incubation at different temperatures by fluorescence microscopy. At 4 °C, internalization of CPT-11lip was almost, completely suppressed; while uptake of CPT-11sol was not affected in the same experimental conditions (see Fig 1B).

Together, these findings indicate that an endocytic process was involved in CPT-11lip internalization while free CPT-11 penetrates across plasma membrane by diffusion. It has been described that liposomes appear to enter cells via an energy-dependent vesicular transport (Torchilin, 2005).

3.3. Selective cytotoxicity against HeLa cells

The cytotoxic effectiveness liposomal-CPT-11 was also assessed and compared with that of the free drug. Cell proliferation was evaluated by the MTT colorimetric assay. Hs68 and HeLa cells were treated with CPT-11lip and CPT-11sol for 48 h and measures were carried out immediately (0), 24 and 48 h after drug removal.

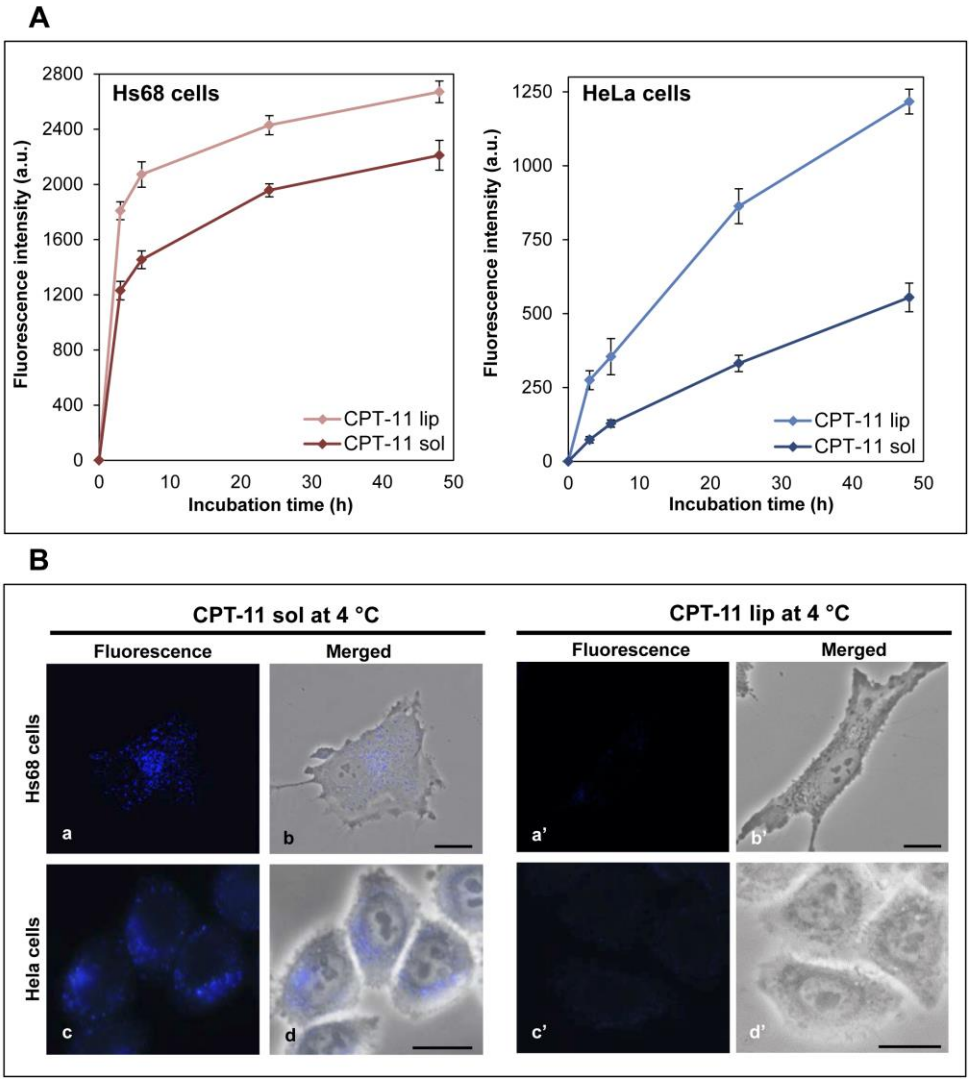

Fig 1. Uptake and mechanisms of cell entry of CPT-11sol and CPT-11lip into Hs68 and HeLa cells. A) The graphs show the quantitative analysis of the internalization of CPT-11 in Hs68 (a) and HeLa (b) cells carried out by flow cytometry. Cells were incubated with 100 µM CPT-11lip (light symbols) or 100 µM CPT-11sol (dark symbols) for different periods of time, at 37 °C. Emission fluorescence at 450 nm was determined after excitation at 405 nm. Data are the means ± SD from three different experiments. Significance was assessed using a Student's paired t-test, being P<0.0014 and P<0,018 for Hs68 and HeLa cells, respectively. B) Incubations with CPT-11lip and CPT-11sol for 3 h at 4 °C visualized by fluorescence (UV excitation) and merged images with phase-contrast microscopy. (a, b) Hs68 cells incubated with CPT-11sol. (c, d) HeLa cells incubated with CPT-11sol. (a', b') Hs68 cells incubated with CPT-11lip. (c', d') HeLa cells incubated with CPT-11lip. Scale bar: 10 µm.

Fig 2 (A and B) shows reduced values obtained in the MTT assay for CPT-11 treated cells in relation to control cells depending on time elapsed after the end of treatment in both cell lines. Also, survival rates in both cell lines were lower for CPT-11lip in comparison with CPT-11sol at all post-incubation times analyzed. Results of MTT assay in Hs68 cells were different in those regarding to the percentage of cell survival. In the case of Hs68 cells the survival significantly decreases from 100 to 40% when incubated with CPT-11lip and after 48 h of drug removal.

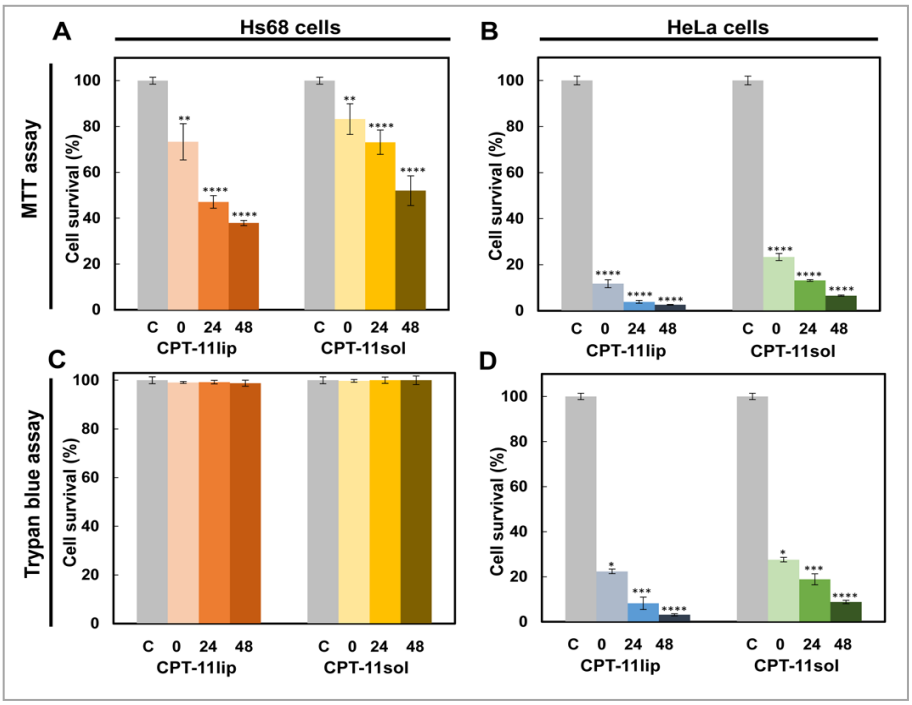

Fig 2. Cell survival at different times (0, 24 and 48 h) after CPT-11 removal. (A, B) Surviving fraction of Hs68 and HeLa cells incubated 48 h with 100 µM CPT-11lip or CPT-11sol evaluated by MTT assay, respectively. (C, D) Surviving fraction of Hs68 and HeLa cells measured by Trypan blue assay, respectively. Data correspond to mean values ± standard deviation from at least eight different experiments for MTT assay and four different experiments for Trypan blue assay.

On the contrary, HeLa cells survival decreased with time elapsed after the end of the CPT-11lip treatment from 100 to 3%, indicating the high cytotoxicity induced by CPT-11lip on this cell line. Furthermore, toxicity of liposomes without CPT-11 was assessed by MTT assay. Empty liposomes showed no toxicity in both Hs68 and HeLa cells. Surviving fractions of 92.5 ± 3.5% and 93.8 ± 3.1% were obtained in Hs68 and HeLa cells, respectively.

Trypan blue exclusion test was also employed in both cell lines to validate MTT results (Fig 2 C and D). When the assay was carried out with Hs68 cells, the viability was greater than 97% after treatment for all elapsed times (no significant differences). Therefore, CPT-11 seems to induce an anti-proliferative activity without causing cell death on Hs68 fibroblasts. Interestingly, Fig 2D shows that Trypan blue assay results on HeLa cells, were in total accordance with those of the MTT test, being the results of CPT-11lip and CPT-11sol significantly different (Fig 2D).

In summary, Hs68 cells showed a large difference between data from MTT and Trypan blue assays. MTT results reflected a reduction of the proliferation of Hs68 cells due to the effect of CPT-11lip. However, Trypan blue exclusion test showed viability data higher than 97%. These data emphasize the need of using different methods to determine the effect of new agents or therapies on cell viability to avoid generating misleading results (Rello-Varona *et al.*, 2015).

Wei *et al.* (2013) have also reported a study about the preparation and evaluation of two CPT-11 liposomal formulations, although the *in vitro* assessment of their cytotoxic effect on four different tumor cell lines gives quite different results from those described in our study. It should be noted, however, some significant differences that hinder the establishment of valid comparisons between the results of both studies. The different lipid composition used in the design of the carrier, the heterogeneous sized procured liposome populations and the experimental conditions and methodology used by Wei *et al.* (2013). Related to these comments, there are some interesting considerations made by Perche and Torchilin (2013). The authors emphasize on the influence of lipid composition on the release and internalization, endosomal escape strategies and mitochondria targeting when anticancer drugs where formulated in liposomal delivery carriers. In addition, it has also been demonstrated that the efficiency of cellular uptake and the subsequent intracellular processing of liposomes is influenced by both their size and surface characteristics (Andar *et al.*, 2014).

Finally, results of several assays performed in our study with empty liposomes (without CPT-11) evidenced their high degree of biocompatibility and have been incorporated in Supporting Information (see Figs S2 and S3).

3.4. Endosomal localization of CPT-11lip in HeLa and Hs68 cells

As can be observed in Fig 3B, after 24 h incubation with CPT-11lip (100 μM), a similar localization pattern was detected in both cell lines. Blue fluorescence was mainly localized as a granular pattern dispersed in the cytoplasm near the nucleus in HeLa and Hs68 cells. Subcellular localization in the endosomal compartment was confirmed with LysoTracker Red DND-99 (Fig 3B, c and g). The blue CPT-11 signal co-localizes with the red fluorescence of the labelled endosomes in both cell lines (Fig 3B, d and h) indicating that endosomal acidic compartment was the main site of CPT-11lip accumulation. Subsequently, CPT-11 would be released from this site to reach the nucleus in order to exert their cytotoxic effect as Topo I poison.

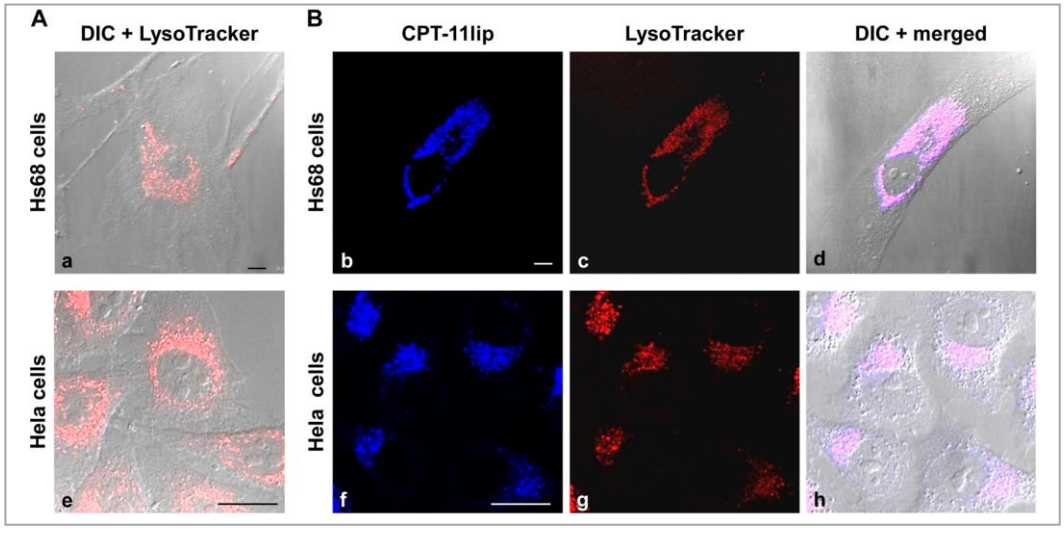

Fig 3. Analysis of the CTP-11lip localization**.** A) (a,e) Confocal microscopy fluorescence images of LysoTracker® Green under blue exciting light, merged with differential interference contrast (DIC) microscopy of control Hs68 and HeLa cells, respectively. B) Cells were treated with CPT-11lip (100 μM) for 24 h and counterstained with LysoTracker® Red DND-99, before being observed by DIC and confocal microscopy. (b-d)

Hs68 cells show blue fluorescent spots in the cytoplasm that almost completely co-localize with LysoTracker® Red. (f-h) HeLa cells show a similar subcellular distribution pattern. Scale bars: 10 μm.

There are relatively few studies related to the subcellular localization of CPT derivatives and the published results are somewhat heterogeneous. For instance, water-soluble topotecan has been mainly localized in mitochondria within HT-29 cells (Croce *et al.*, 2004) and in nuclei in MCF-7 breast tumor cells line (Errington *et al.*, 2005), whereas lipophilic gimatecan exhibited a lysosomal localization in HT-29 cells (Croce *et al.*, 2004). These results indicate a quite different behavior of these CPT derivatives and suggest that subcellular distribution plays an important role in their cytotoxic potency. Localization in the endosomal-lysosomal compartment could contribute to the drug potency, because lysosomes represent a store allowing intracellular release of active drug (Croce *et al.*, 2004). In a similar way, namitecan, a hydrophilic CPT derivative whose clinical development is currently ongoing, has been shown to accumulate in lysosomes of both A431 and A431/TPT (resistant to topotecan) cells (Zuco *et al.*, 2010).

3.5. CPT-11lip induces morphological changes in HeLa cells but not in Hs68 cells

The next step was to analyze the time course (0, 24 and 48 h after CPT-11lip removal) of the morphological changes after treatment with 100 μM CPT-11lip, in both cell lines, by toluidine blue staining. As shown in Fig 4A, Hs68 fibroblasts treated with CPT-11lip did not show any alteration in cell morphology, being the cells attached to the plates, although almost a complete absence of mitotic figures was detected. Starting from plates with the same number of seeded Hs68 cells, the cellular density after incubation with the drug did not increase as compared to non-treated control cells. Therefore, Hs68 fibroblasts seem to lose the ability to replicate during their treatment with CPT-11lip.

On the contrary, HeLa cells showed significant morphological changes, depending on time elapsed after the end of CPT-11lip treatment. As can be seen in Fig 4B, after 0, 24 and 48 h of drug removal the cell density was considerably lower compared to control cultures and the great majority of cells (95%) became detached from the plates and appeared as floating cells in the culture medium, showing an altered cell shape with large and lateralized nucleus. Furthermore, 24 and 48 h after treatment, the few HeLa cells still attached to the plates were larger and flatter than control cells and had long cytoplasmic projections. Based on these morphological results, we hypothesized that in response to CPT-11lip treatment, apoptosis was triggered in detached HeLa cells, whilst attached cells showed long and thin cellular extensions.

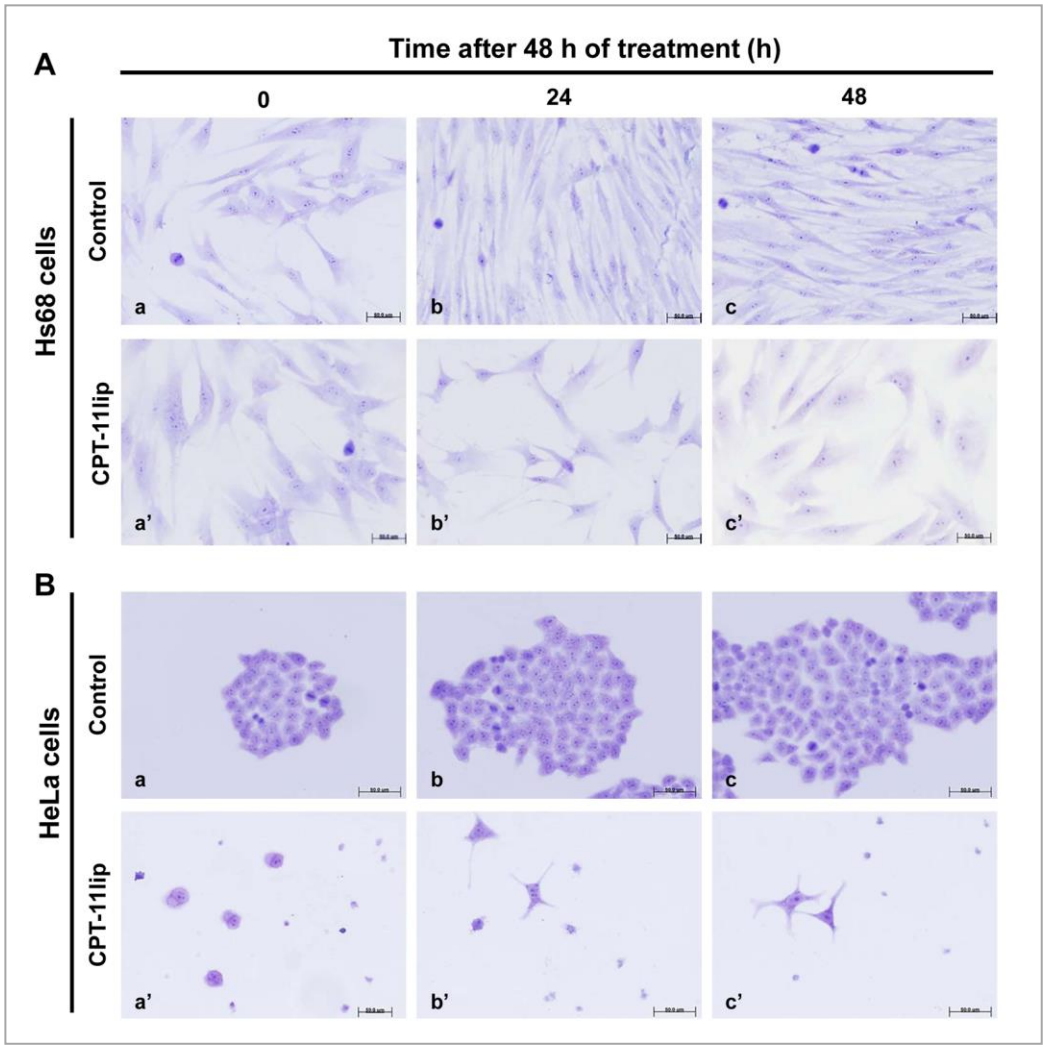

Fig 4. Morphological changes after treatment**.** Cell morphology visualized by toluidine blue staining immediately, 24 and 48 h after CPT-11lip treatment. A) Analysis of Hs68 cells. (a-c) Untreated (control) Hs68 cells. (a'-c') Treated Hs68 cells: CPT-11lip did not cause loss of cell adhesion or cell morphology changes in Hs68 cells at different times after incubation. B) Analysis of HeLa cells. (a-c) Control HeLa cells. (a'-c') Treated HeLa cells: the vast majority of HeLa cells were detached from plastic after CPT-11lip incubation. Note that the few remaining adherent cells changed their shape and size.

To our knowledge similar studies have not been described previously for any CPT derivative. Several studies have shown that CPT-11 incorporated into liposomes is more effective than the free drug (Ramsay *et al.*, 2008; Carnevale and Ko, 2016). Recent reviews have highlighted important advantages of liposomal formulations of chemotherapeutic agents, with an increased efficacy and reduced toxicity compared to un-entrapped drugs in cancer therapy (Perche and Torchilin, 2013; Allen and Cullis, 2013).

The different cell line sensitivity to CPT-11lip is in agreement with previous data in the literature. Rudolf *et al.* (2012) reported that CPT-11 induces apoptosis in normal colonic epithelial cells, whereas premature senescence was the prevalent response in normal colonic fibroblasts from mesenchymal origin. Also, the authors analyze the CPT-11 cytotoxic effects against HCT-116 cells (human colorectal carcinoma cell line). Comparing our results with those reported by the authors, liposomes appear to serve as an effective carrier system for CPT-11 delivery, since using equal exposure time (48 h), quarter-doses (100 μM *vs.* 250 μg/ml ≈ 370 μM) are required to kill a greater percentage of tumor cells (90% Hela cells *vs*. 73% HCT-116 cells).

3.6. CPT-11lip triggers massive apoptosis in Hela cells

LDH activity in the culture medium of CPT-11lip treated HeLa cells and Hs68 fibroblasts was the same as that present in the culture medium of controls (Fig 5A), indicating that the

cytosolic membrane of both cell lines conserves its integrity after drug exposure and allows to discard the involvement of necrotic processes.

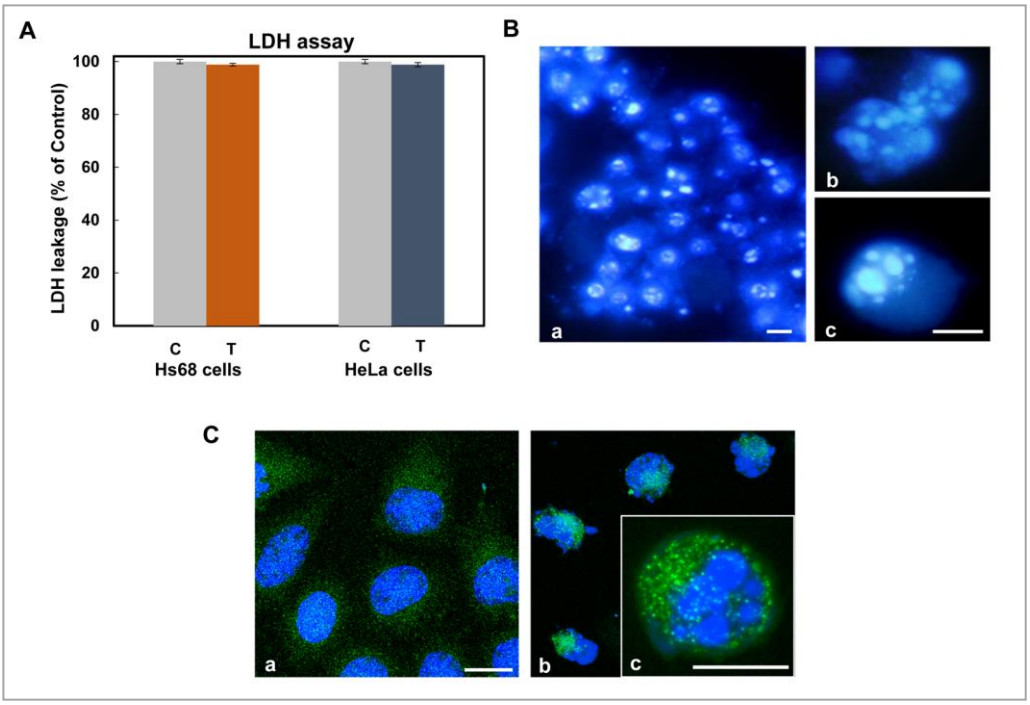

Fig 5. Identification of apoptotic HeLa cells death induced by 100 µM CPT-11lip. A) LDH assay results. Statistical analysis showed that there was no significant difference between the control (C) and CPT-11lip treated (T) cells. B) Detached HeLa cells after 48 h of incubation with liposomal CPT-11 stained with H-33258. (a) Low magnification. (b, c) Images taken at a higher magnification. Scale bars 10 µm. C) Confocal fluorescence merged images of HeLa cells visualized by Bax immunofluorescence (green) and H-33258 counterstaining of nuclei (blue). (a) Control cells with diffuse Bax signal in the cytosol. (b) Images of translocation of Bax protein from the cytosol into mitochondria of HeLa cells. Scale bars: 10 µm. (c) Apoptotic cell at higher magnification.

Detached HeLa cells stained with H-33258 after 48 h of incubation with CPT-11lip, showed typical apoptotic features (Fig 5B). Cells became rounded with chromatin condensed and fragmented, and packed into apoptotic bodies.

The involvement of mitochondrial apoptotic pathway as the main mechanism of HeLa cell death after treatment with CPT-11lip was supported by indirect immunofluorescence staining of diffuse green cytoplasmic fluorescence for Bax around the blue nuclear emission by H-33258 (Fig 5C, a) (Rello-Varona *et al.*, 2015). In contrast, immediately after treatment with CPT-11lip an increased intensity of the green signal for Bax, concentrated in structures corresponding to mitochondria, could be observed in the few attached HeLa cells (Fig 5C, b

and c). In addition to the relocation of the Bax protein, these cells showed nuclei with condensed and fragmented chromatin (H-33258 staining).

Furthermore, the analysis of images obtained under the inverted microscope and performed at different times of evaluation (before and after 48 h treatment), showed that the incubation with empty liposomes did not produce morphological alterations. On the contrary, after 48 h of CPT-11lip treatment, the few cells that were still attached to the culture substrate showed apoptotic characteristics (see Fig S3).

3.7. Different responses of CPT-11lip in both cell lines related to cell cycle and senescence

Taking into account the different cytotoxic responses of Hs68 and HeLa cells to CPT-11lip, we proceeded to analyzed different physiological cellular parameters that might be involved in the different behavior of both cell types.

First, we analyzed the effects on cell cycle phase distribution on both cell lines, immediately, 24 and 48 h post-treatment after treatment with 100 µM CPT-11lip for 48 h. As can be seen in Fig 6 A and B, we detected that CPT-11lip induced a marked G2/M arrest and polyploidization in HeLa cells, but not in Hs68 cells.

For Hs68 fibroblasts, the amount of cells in the sub G1 phase (apoptotic cell population), after CPT-11lip treatment, was negligible and aneuploidization-tetraploidization (> 4C) was only slightly and transiently promoted after CPT-11lip removal. 24 h after withdrawing the drug an increase in the percentage of cells in S and G2/M phases (29% and 20%, respectively) was detected in Hs68 cells. However, after 48 h, these values were reduced to 18% and 7%, respectively. Moreover, 24 h after drug removal, a significant decrease of the G0/G1 phase (42%) was observed but a new increase in the percentage of this cell cycle phase (62%) was obtained after 48 h post-treatment.

On the contrary, HeLa cells (Fig 6B) cycle kinetics following CPT-11lip showed: i) a significant increase of the peak placed in the sector corresponding to apoptotic cells (sub G1); ii) a cell cycle arrest in G2/M, with a maximum value at 24 h, and iii) a progressive polyploidization of HeLa cells (42%) at 48 h after withdrawing CPT-11lip. It is important to note that results related to cell cycle changes in both cell lines were consistent with morphological, cytotoxic and apoptotic assays mentioned above.

In order to test if senescence was triggered in attached HeLa cells and in non-proliferating Hs68 cells after incubation with CPT-11lip, we carried out the β-galactosidase assay at different elapsed times (2 and 5 days) after drug removal. Senescent-associated β-galactosidase (SA-β-gal) cells can be visualized as a blue perinuclear staining under phase contrast microscopy. SA-β-gal positive cells were counted and their amount was referred to the total number of cells on the plate (Fig 6C).

Hs68 cells appear to enter in a quiescent state only as a transient response and the percentage of positive SA-β-gal Hs68 cells was reduced from 72%, when the drug was removed, until 12% after five days of its removal, but without enlarged cell size (Fig 6D).

By contrast, the surviving HeLa cells after treatment with CPT-11lip, though few and clearly r**ec**ognizable as tetraploid cells because of its increased size, had higher records of senescent response than Hs68 fibroblasts. The quantitative results show that the percentage of senescent HeLa cells increased progressively with the time elapsed after the removal of the drug, being 92.6% within five days. In summary, our results indicate that some HeLa cells can survive after treatment with CPT-11lip, remaining in a state of senescence, whereas Hs68 fibroblasts temporarily enter a growth arrest but they become proliferative cells again after drug withdrawal.

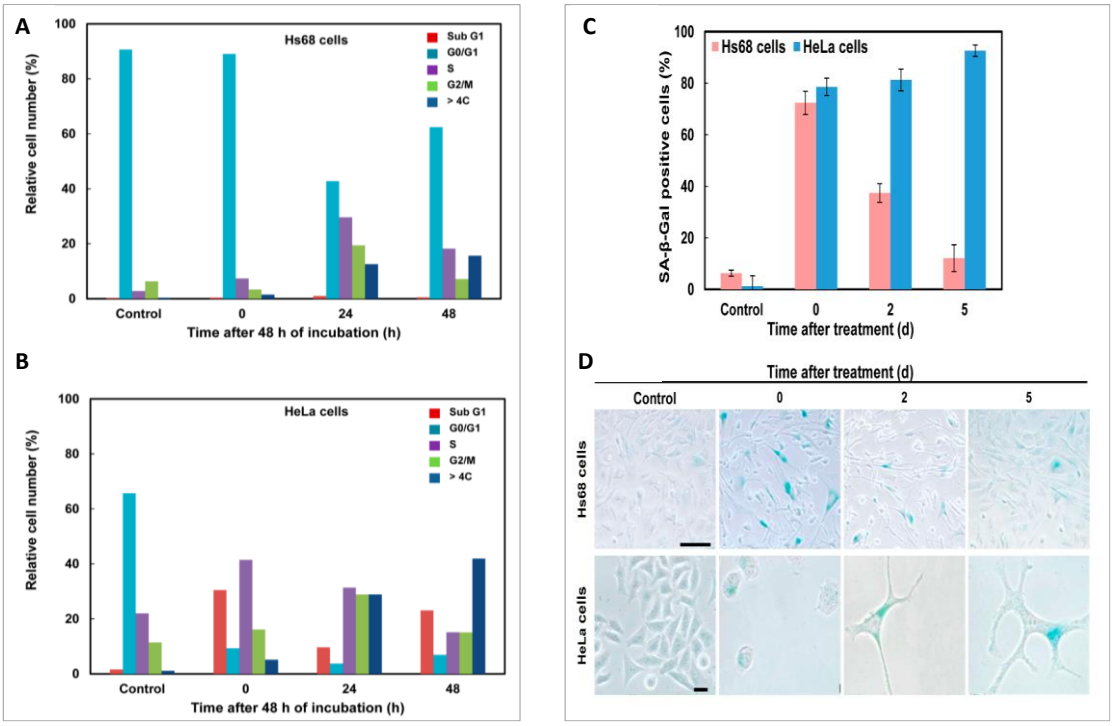

Fig 6. Cell cycle analysis and senescence-associated β-galactosidase assay. (A, B) Effects of CPT-11lip on cell cycle phase distribution on Hs68 and HeLa cells, respectively. Results were obtained from two independent experiments. For each experiment, a minimum of 20 000 events were analyzed. (C) Cellular senescence-associated β-galactosidase activities at 0 (immediately), 2 and 5 days after incubation. Percentages of senescent cells referred to the total amount of cells on the plate. Results are the mean of three different experiments ± SD. (D) Images correspond to a representative assay. Scale bars: 10 µm.

Therefore, these results may reflect that Hs68 suffered a temporary and reversible entry in cell cycle arrest, different to senescence as proposed by Blagosklonny (2011). On the contrary, at the same time interval after drug removal, scarce HeLa cells can survive after treatment with CPT-11lip, remaining still attached to the substrate, being positive for SA-β-gal and showing a senescent phenotype. Our findings in HeLa cells are consistent with those of Haug *et al.* (2008) in human colon cancer cell lines: G2/M arrest, growth inhibition, polyploidization, cell death (96 h after treatment), and senescence phenotype in two cell lines, treated with CPT-11.

3.8. Effect of CPT-11lip on p53, Bax and Bcl-2 mRNA expression profiles

Finally, the expression levels of *TP53* (p53), *BAX* (Bax) and *BCL-2* (Bcl-2) mRNA at 3, 6, 24 and 48 h after incubation of Hs68 and HeLa cells with CPT-11lip were studied by real-time

PCR. As shown in Fig 7A, time-course experiments revealed that in Hs68 cells, p53 expression was slightly but significantly induced in treated cells compared with untreated control cells at 3 and 48 h after CPT-11lip incubation. Regarding the expression of Bax mRNA, no significant changes were detected at the different time intervals post-treatment analyzed. On the contrary, mRNA induction of Bcl-2 was significantly down-regulated after 6, 24 and 48 h of CPT-11lip treatment, compared to control Hs68 cells (without CPT-11lip treatment). In HeLa cells, p53 mRNA expression was also up-regulated from 3 until 24 h compared with control (Fig 7B). Furthermore, our results of RT-PCR indicated that in the response of HeLa cells to CPT-11lip, a drastic decrease in expression level of Bcl-2 was produced after 3 h of incubation with a slight but significant increase in Bax expression after 48 h of treatment. These results are consistent with massive apoptotic induction.

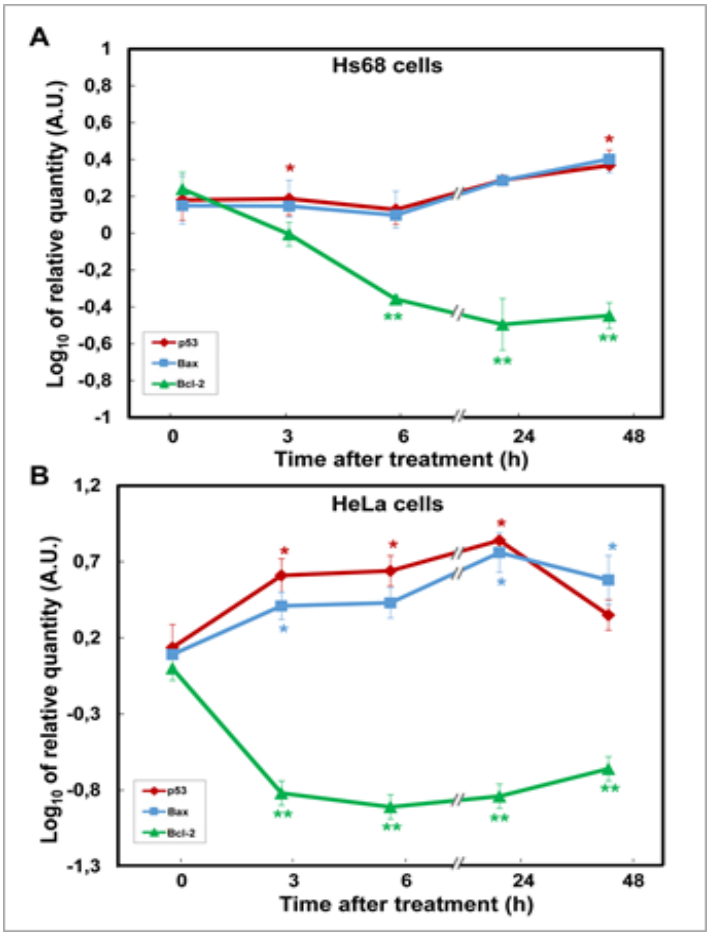

Fig 7. Time-dependent effects of incubation with CPT-11lip on mRNA expression levels of p53, Bax and Bcl-2 by real-time PCR assay. A) RT-PCR in Hs68 cells. B) RT-PCR in HeLa cells. GAPDH mRNA was used as an internal control. Results are represented as the log10 of the relative quantity normalized to control cells. Data are means ± SD from at least three different experiments. Significance was assessed using Student's t test: *P<0.05, and **P<0.005.

Our results related to mRNA levels of p53 in Hs68 cells indicated that the temporary cell arrest in Hs68 cells did not imply the continuous increase in p53 expression levels. In this sense, Michishita *et al.* (1998) have described that inhibitors of DNA topoisomerases induced arrest in cell division in human embryonic fibroblasts with SA-β-gal and without changes in p53 expression, but with cell growth upon inhibitors removal. Several publications have reported a p53-dependent senescence program in response to DNA damaging agents in different types of cells (Rudolf *et al.*, 2012; Kim *et al.*, 2015). On the other hand, CPT-11lip induced in HeLa cells a massive apoptotic response, which seems not being related to p53 status. It is well known-that HeLa cells express wild-type p53, but the protein product is human papillomavirus inactivated and rapidly degraded (Kralj *et al.*, 2003), so DNA damage in these cells could not be repaired, and a p53-independent apoptotic route was triggered by CPT-11lip on HeLa cells. These findings agree well with other published results (Shao *et al.*, 2001; Rudolf *et al.*, 2011), so CPT seems to trigger apoptosis through p53-dependent and -independent pathways.

3.9. Cytoskeleton organization of cells treated with CPT-11lip

To get additional insight into the global mechanism of inactivation of both cell lines underlying CPT-11lip cellular responses, the effects of incubation with CPT-11lip on the organization and distribution of F-actin microfilaments and on vinculin, a focal adhesion-associated protein, at different post-incubation times (0, 24 and 48 h), were investigated.

Fig 8 shows the sequence of events related to F-actin microfilaments and vinculin, leading to the death of HeLa cells by apoptosis and a reversible cell cycle arrest with temporary absence of proliferation of Hs68 cells. Confocal microscopy analysis of Hs68 samples revealed that

CPT-11lip did not show, at all times selected, any alteration on F-actin and vinculin, which appeared at both ends of stress fibers as part of the focal adhesion, similar to control cells (see Fig 8A).

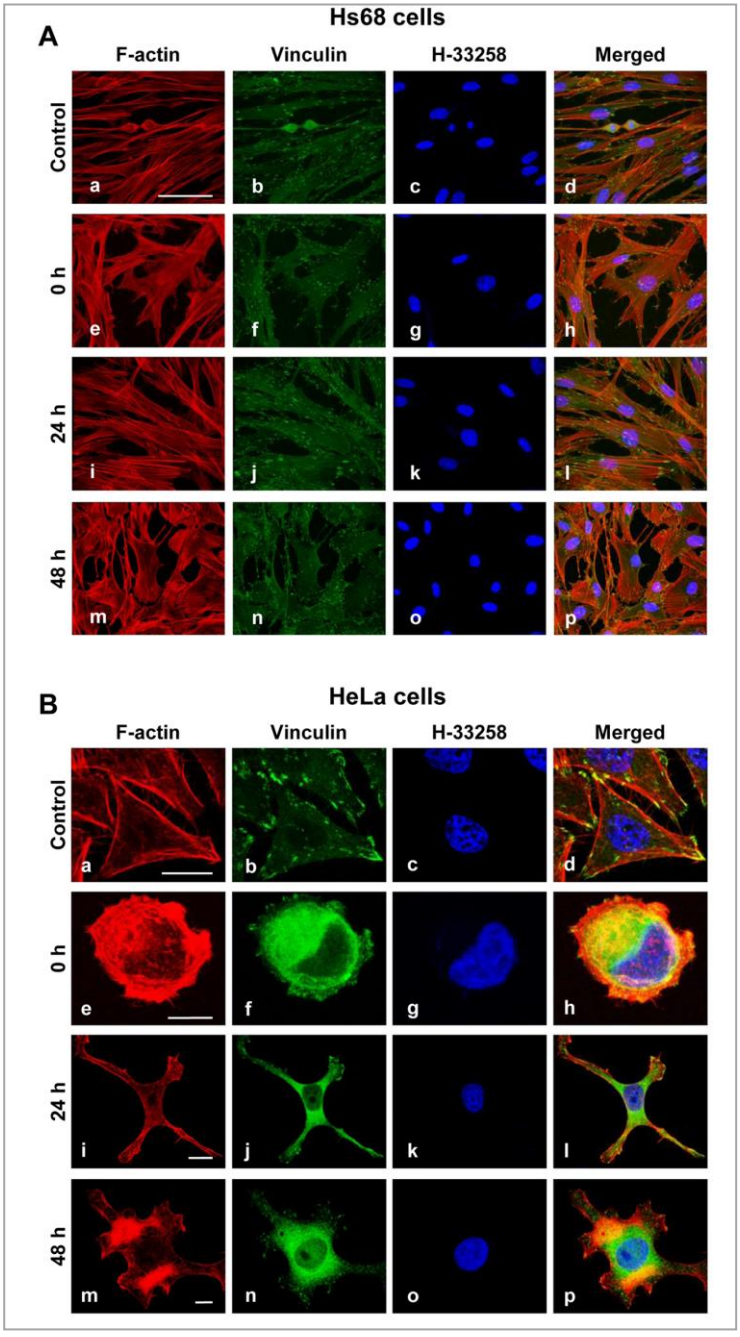

Fig 8. F-actin and vinculin in Hs68 and HeLa cells after incubation with CPT-11lip. A) Cytoskeleton confocal images of Hs68 cells observed in control (a-d) and immediately, 24 or 48 h (e-p) after drug removal, respectively. B) The same analysis was performed in HeLa cells. F-actin structures are shown in red (stained with phalloidin-

TRITC), green corresponds to immunolabelling of vinculin, the blue signal refers to chromatin (stained with H-33258), and last column to overlay images. The cells shown in each panel are representative of predominant morphologies observed in four separate experiments. Scale bars: 20 μm.

On the contrary, attached HeLa cells at the end of treatment exhibited profound changes either in cell size and morphology, as well as in F-actin distribution, throughout the different time points studied (see Fig 8B). Immediately after drug removal, attached HeLa cells presented a completely disorganized F-actin cytoskeleton with a dramatic increase in the vinculin signal and a partial cell rounding, which might represent an obstacle for the cell adhesion to substrate. As time goes by, attached HeLa cells suffered other morphological changes and 24 h after drug removal, cells showed long extensions, like large filopodia, containing F-actin. These results directly correlate to the morphological changes observed on HeLa cells with toluidine blue staining (see Fig 4). Likewise, 48 h after CPT-11lip treatment actin stress fibers and vinculin in focal adhesion were still found.

It is also important to note the general increase in size of cells, at the same time as the cell nucleus grows to almost 30 μm and its location in the cell is polarized.

These results were not surprising, since changes in size and cell morphology in attached HeLa cells must be due to cytoskeleton reorganisation. In this respect, cytoskeleton of senescent cells has been mainly studied using senescent and young skin fibroblasts. It has been reported that senescent cells developed a long and dense vimentin network, long and thin actin fibres, and numerous small focal contact sites (Nishio and Inoue, 2005).

3.10. Different cell line response to DNA damage

As part of our efforts to unravel CPT-11lip's mechanisms of action, we examined DNA double-strand breaks (DSBs) accumulation at different times (3, 6, and 24 h) after CPT-11lip incubation by immunodetection of the phosphorylated histone gamma-H2AX (Fig 9). It is well known that the phosphorylation of histone H2AX at serine 139 (γ-H2AX) is the most sensitive

molecular marker of DNA damage and repair in cells exposed to ionizing radiation or DNA-damaging chemotherapeutic drugs, given its specificity and sensitivity (Sharma *et al.*, 2012).

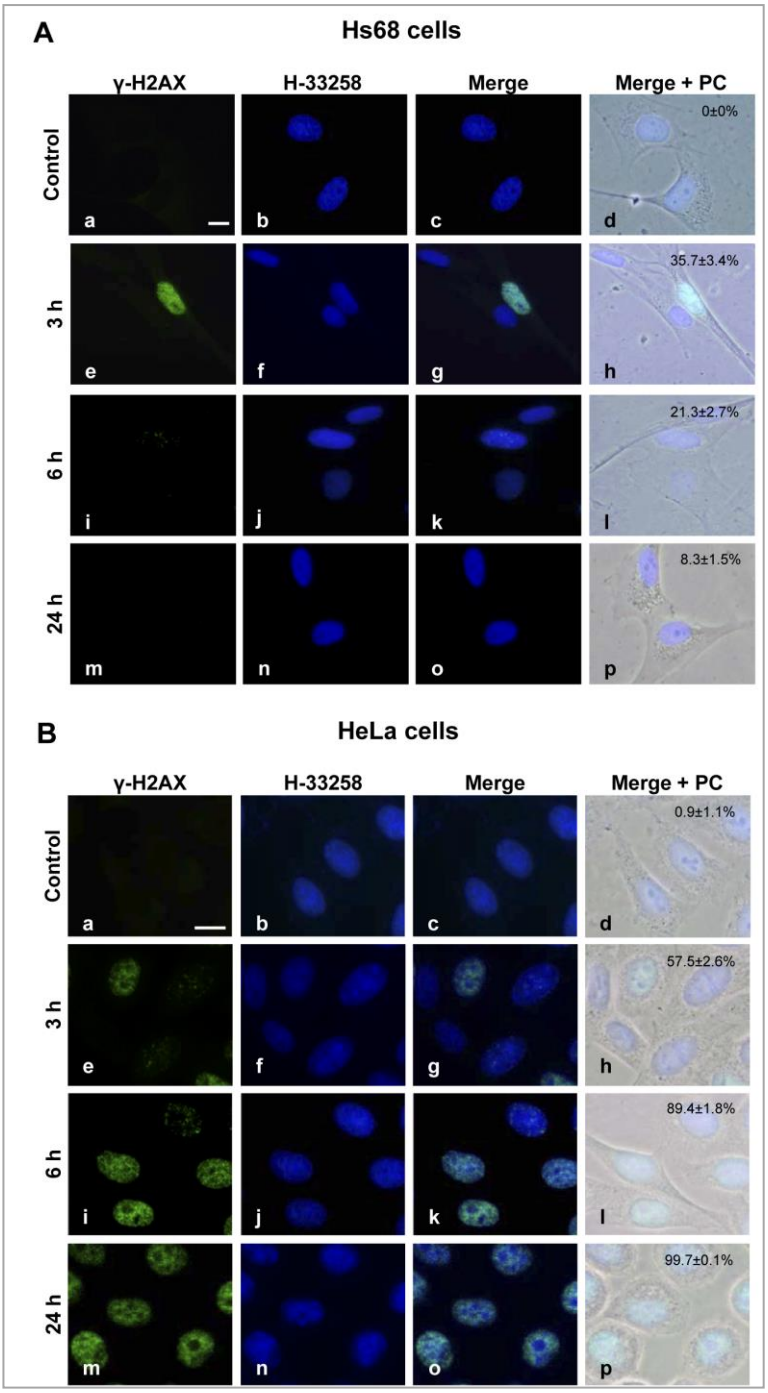

Fig 9. Immunofluorescent analysis of γ-H2AX. A) Representative images of Hs68 cells immunostaining to H2AX γ-phosphorylated histone (green), counterstained with H-33258 (blue), merged images and overlay of fluorescence and phase-contrast microscopy (PC) at three different incubation times with CPT11-lip. (a-d) Control Hs68 cells. (e-h), (i-l), (m-p) Cells after 3, 6 and 24 h of incubation, respectively. B) Representative images of HeLa cells under the same experimental conditions. Scale bars: 10 μm. The percentage of cells positive for γ-

H2AX immunofluorescence has been included in the images of the right column. Values represent means ± standard deviation of three independent experiments in which at least 200 cells were counted for each experimental condition.

As can be seen, an accumulation of DNA damage over time was detected in HeLa cells (Fig 9B). On the contrary, the results obtained in Hs68 cells suggested that normal cells were able to repair CPT-11 induced DNA damage (Fig 9A). These results are specific for CPT-11lip, as empty liposomes did not significantly induce DNA damage (see Fig S2). The percentage of cells positive for γ-H2AX immunofluorescence revealed DNA damage of Hs68 cells at 3 h incubation with CPT-11lip. However, the percentage of positive cells was significantly reduced at 6 and 24 h of CPT-11lip administration. On the other hand, the percentage of positive HeLa cells was rapidly increased following exposure to CPT-11lip and virtually 100% of HeLa cells were positively labeled at 24 h of incubation. These results indicate that CPT-11 formulated in liposomes is capable of reach the cell nucleus after its release from carrier (liposomes), exerting a cytotoxic effect on HeLa cells but not in non-transformed Hs68 cells.
Similar to our findings, Tamura *et al.* (2012) evaluated the effect of three Topo I inhibitors (camptothecin, CPT-11 and SN-38) using cultures of 15 cell lines of human tumors and normal cells, and all Topo I poisons were shown to be more cytotoxic for tumor cell lines than for normal mesenchymal and epithelial cells.

Taken together, these results indicate that liposomes possess the following *in vitro* properties for the success of CPT-11 delivery: i) liposomes demonstrated both stability and high encapsulation efficiency, as well as biocompatibility (without CPT-11); ii) CPT-11lip were efficiently internalized by an endocytic process into both cell lines with a lysosomal subcellular accumulation; iii) CPT-11lip was not cytotoxic to normal fibroblast Hs68 cells, but induced a massive apoptosis, accompanied by cell senescence, in HeLa cells; iv) CPT-11 can be released from lysosomes and reach the cell nucleus; and v) DNA damage triggers different cellular

responses: a p53-dependent Hs68 cell survival and a p53-independent apoptotic response in HeLa cells.

These remarkably different responses might constitute the basis for a promising approach to reduce the side effects associated to CPT-11 treatments. Anyhow, assessment of chemotherapeutic potential of new pharmaceutical formulations requires a detailed knowledge of its underlying mechanism of action, as a first step in the pharmacological study of the drug, by means of *in vitro* experiments with cell cultures before the *in vivo* assays (He et al., 2017). In addition, new studies to identify the different signaling pathways triggered by CPT-11lip in these and other cell types will be performed before long. If the results are as expected, experimental assays *in vivo* will be then carried out.

Conclusions

The development of new anticancer drug delivery systems has undergone a spectacular development over the last years, and a variety of nanocarriers, including liposomal devices, are being tested. Here, we present a comparative study of the cytotoxic effects induced by CPT-11 encapsulated into liposomes in two human cell lines: HeLa (cervix adenocarcinoma) and Hs68 (foreskin fibroblasts). Our findings indicate that phospholipid-cholesterol liposomes possess optimum properties in order to be considered as suitable CPT-11 carriers. To our knowledge, it is the first time that a deep and multiparametric research (subcellular localization, cytotoxic effect and activation of signaling pathways) has been carried out using two cell lines with different gene profiles, justifying a chemotherapeutic drug (CPT-11) formulation in liposomes.

Acknowledgements

This work was supported by the Spanish Ministry of Economy and Competitiveness (grant numbers CTQ2013-48767-C3-1-R, CTQ2013-48767-C3-3-R), Comunidad de Madrid (S2013/MIT-2850) and Govern de la Generalitat de Catalunya (2009SGR-367). A. Casadó

thanks to the University of Barcelona for a predoctoral fellowship and P. Acedo gratefully acknowledge postdoctoral fellowship support from the Ramón Areces Foundation. We recognise the valuable contribution of Sylvia Gutiérrez (Confocal Microscopy, Centro Nacional de Biotecnología, Madrid).

References

Allen, M.T., Cullis, P.R., 2013. Liposomal drug delivery systems: From concept to clinical applications. Adv. Drug. Deliv. Rev. 65, 36-48. doi: 10.1016/j.addr.2012.09.037

Andar, A.U., Hood, R.R., Vreeland, W.N., DeVoe, D.L., Swaan, P.W., 2014. Microfluidic Preparation of Liposomes to Determine Particle Size Influence on Cellular Uptake Mechanisms. Pharm. Res. 31, 401-413. doi: 10.1007/s11095-013-1171-8

Arancia, G., Calcabrini, A., Matarrese, P., Marcocci, L., Pietrangeli, P., Mondovi, B., 1994. Effects of incubation with liposomes at different temperatures on cultured melanoma cells (M14). Int. J. Hyperthermia 10, 101–114. doi: 10.3109/02656739409009336

Bai, L., Zhu, W-G., 2006. p53: Structure, function and therapeutic applications. J. Cancer Mol. 2, 141-153.

Ben-Porath, I., Weinberg, R.A., 2005.The signals and pathways activating cellular senescence. Int. J. Biochem. Cell Biol. 37, 961-976. doi: 10.1016/j.biocel.2004.10.013

Bhonde, M.R., Hanski, M-L., Notter, M., Gillissen, B.F., Daniel, P.T., Zeitz, M., Hanski, C., 2006. Equivalent effect of DNA damage-induced apoptotic cell death or long-term cell cycle arrest on colon carcinoma cell proliferation and tumour growth. Oncogene 25, 165-175. doi: 10.1038/sj.onc.1209017

Blagosklonny, M.V., 2011. Cell cycle arrest is not senescence. Aging 3, 94-101. doi: 10.18632/aging.100281

Bozzuto, G., Molinari, A., 2015. Liposomes as nanomedical devices. Int. J. Nanomedicine 10, 975-999. doi: org/10.2147/IJN.S68861

Burke, T.G., Gao, X., 1994. Stabilization of topotecan in low pH liposomes composed of distearoylphosphatidylcholine. J. Pharm. Sci. 83, 967-969. doi: 10.1002/jps.2600830710

Burke, T.G., Bom, D., 2000. Camptothecin design and delivery approaches for elevating anti-topoisomerase I activities in vivo. Ann. NY Acad. Sci. 922, 36-45. doi: 10.1111/j.1749-6632.2000.tb07023.x

Carnevale, J., Ko, A.H., 2016. MM-398 (nanoliposomal irinotecan): emergence of a novel therapy for the treatment of advanced pancreatic cancer. Future Oncol. 12, 453-464. doi: 10.2217/fon.15.333

Casadó, A., Sagristá, M.L., Mora, M., 2014. Formulation and in vitro characterization of thermosensitive liposomes for the delivery of irinotecan. J. Pharm. Sci. 103, 3127-3138. doi: 10.1002/jps.24097

Casadó, A., Giuffrida, M.C., Sagristá, M.L., Castelli, F., Pujol, M., Alsina, M.A., Mora, M., 2016. Langmuir monolayers and Differential Scanning Calorimetry for the study of the interactions between camptothecin drugs and biomembrane models. Biochim. Biophys. Acta 1858, 422-433. doi: 10.1016/j.bbamem.2015.12.007

Chen, A.Y., Liu, L.F., 1994. DNA topoisomerases: Essential enzymes and lethal targets. Annu. Rev. Pharmacol. Toxicol. 34, 191-218. doi: 10.1146/annurev.pa.34.040194.001203

Chu, E., 2012. An update to the current and emerging targeted agents in metastatic colorectal cancer. Clin. Colorectal Cancer 11, 1-13. doi: 10.1016/j.clcc.2011.05.005 16

Chustecka, Z., 2015. Liposomal Irinotecan (MM-398) Approved in Pancreatic Cancer. Medscape Oct 22. http://www.medscape.com/viewarticle/853072 (accessed 15.10.22)

Croce, A.C., Bottiroli, G., Supino, R., Favini, E., Zuco, V., Zunino, F., 2004. Subcellular localization of the camptothecin analogues, topotecan and gimatecan. Biochem. Pharmacol. 67, 1035-1045. doi: 10.1016/j.bcp.2003.10.034

De Jong, W.H., Borm, P.J., 2008. Drug delivery and nanoparticles: Applications and Hazards. Int. J. Nanomedicine 3, 133-149.

Deshpande, P.P., Biswas, S., Torchilin, V.P., 2013. Current trends in the use of liposomes for tumor targeting. Nanomedicine (Lond) 8, 1-32. doi: 10.2217/nnm.13.118

Diaz-Rubio, E., 2004. New chemotherapeutic advances in pancreatic, colorectal and gastric cancers. Oncologist 9, 282-294. doi: 10.1634/theoncologist.9-3-282

Drummond, D.C., Noble, C.O., Hayes, M.E., Park, J.W., Kirpotin, D.B., 2008. Pharmacokinetics and in vivo drug release rates in liposomal nanocarrier development. J. Pharm. Sci. 97, 4696-4740. doi: 10.1002/jps.21358

Eom, Y-W., Kim, M.A., Park, S.S., Goo, M.J., Kwon, H.J., Sohn, S., Wook-Hwan Kim, W-K., Yoon, G., Cho, K.S., 2005. Two distinct modes of cell death induced by doxorubicin: apoptosis and cell death through mitotic catastrophe accompanied by senescence-like phenotype. Oncogene 24, 4765–4777. doi:10.1038/sj.onc.1208627

Errington, R.J., Ameer-Beg, S.M., Vojnovicb, B., Patterson, L.H., Zloh, M., Smith, P.J., 2005. Advanced microscopy solutions for monitoring the kinetics and dynamics of drug–DNA targeting in living cells. Advanced Drug. Deliv. Rev. 57, 153-167. doi: 10.1016/j.addr.2004.05.005

Estanqueiro, M., Amaral, M.H., Conceicão¸ J., Sousa Lobo, J.M., 2015. Nanotechnological carriers for cancer chemotherapy: The state of the art. Colloids and Surfaces B: Biointerfaces, 126, 631-648. http://dx.doi.org/10.1016/j.colsurfb.2014.12.041

García-Carbonero, R., Supko, J.G., 2002. Current perspectives on the clinical experience pharmacology, and continued development of the camptothecins. Clin. Cancer Res. 8, 641-661.

Gupta, M., Fan, S., Zhan, Q., Kohn, K.W., O'Connor, P.M., Pommier, Y., 1997. Inactivation of p53 Increases the cytotoxicity of camptothecin in human colon HCT116 and breast MCF-7 cancer cells. Clin. Cancer Res. 3, 1653-1660.

Hattori, Y., Shi, L., Ding, W., Koga, K., Kawano, K., Hakoshima, M., Maitani, Y., 2009. Novel irinotecan-loaded liposome using phytic acid with high therapeutic efficacy for colon tumors. J. Control. Release 136, 30-37. https://doi.org/10.1016/j.jconrel.2009.01.013

Haug, K., Kravik, K.L., De Angelis, P., 2008. Cellular response to irinotecan in colon cancer cell lines showing differential response to 5-fluorouracil. Anticancer Res. 28, 583-592. doi: 10.1158/0008-5472.CAN-14-0683

He, R., Du, Y., Ling, L., Ismail, M., Hou, Y., Yao, C., Li, X., 2017. Nanoformulation of dual bexarotene-tailed phospholipid conjugate with high drug loading. Eur. J. Pharm. Sci. 100, 197–204. doi:10.1016/j.ejps.2017.01.012

Hegde, S.R., Manimaran, P., Mande, S.C., 2008. Systemic and targeted therapy for advanced colon cancer. Expert Rev. Gastroenterol. Hepatol. 2, 135-149. doi: 10.1586/17474124.2.1.135

Hind, D., Tappenden, P., Tumur, I., Eggington, S., Sutcliffe, P., Ryan, A., 2008. The use of irinotecan, oxaliplatin and raltitrexed for the treatment of advanced colorectal cancer: systematic review and economic evaluation. Health. Technol. Assess. 12, iii-ix, xi-162. doi: http://dx.doi.org/10.3310/hta12150

Hsiang, Y.H., Hertzberg, R., Hecht, S., Liu, L.F., 1985. Camptothecin Induces Protein-linked DNA Breaks via Mammalian DNA Topoisomerase I. J. Biol. Chem. 260, 14873-14878.

Huang, H.C., Mallidi, S., Liu, J., Chiang, C-T., Mai, Z., Goldschmidt, R., Ebrahim-Zadeh, N., Rizvi, I., Hasan, T., 2016. Photodynamic Therapy Synergizes with Irinotecan to Overcome Compensatory Mechanisms and Improve Treatment Outcomes in Pancreatic Cancer. Cancer Res. 76, 1066-1077. doi: 10.1158/0008-5472.CAN-15-0391

Iyer, R., Croucher, J.L., Chorny, M., Mangino, J.L., Alferiev, I.S., Levy, R.J., Venkatadri, Kolla, V., Brodeur, G.M., 2015. Nanoparticle delivery of an SN38 conjugate is more effective than irinotecan in a mouse model of neuroblastoma. Cancer Lett. 360, 205-212. doi: 10.1016/j.canlet.2015.02.011

Juillerat-Jeanneret, L., Schmitt, F., 2007. Chemical modification of therapeutic drugs or drug vector systems to achieve targeted therapy: Looking for the grail. Med. Res. Rev. 27, 574-590. doi: 10.1002/med.20086

Kaku, Y., Tsuchiya, A., Kanno, T., Nishizaki, T., 2015. Irinotecan Induces cell cycle arrest, but not apoptosis or necrosis, in Caco-2 and CW2 colorectal cancer cell lines. Pharmacology 95, 154-159. doi: 10.1159/000381029

Kim, R.H-, Kang, M.K., Kim, T., Yang, P., Bae, S., Williams, D.W., Phung, S.1., Shin, K.H., Hong, C., Park, N.H., 2015. Regulation of p53 during senescence in normal human keratinocytes. Aging Cell 14, 838-846. doi: 10.1111/acel.12364

Köhne, C-H., Lenz, H-J., 2009. Chemotherapy with targeted agents for the treatment of metastatic colorectal cancer. The Oncologist 14, 478-488. doi: 10.1634/theoncologist.2008-0202

Kralj, M., Husnjak, K., Körbler, T., Pavelić, J., 2003. Endogenous p21WAF1/CIP1 status predicts the response of human tumor cells to wild-type p53 and p21WAF1/CIP1 overexpression. Cancer Gene Therapy 10, 457-467. doi: 10.1038/sj.cgt.7700588

Lamb, Y.N., Scott, L.J., 2017. Liposomal irinotecan: A review in metastatic pancreatic adenocarcinoma. Drugs 77, 785-792. doi: 10.1007/s40265-017-0741-1

Liew, S.T., Yang, L.Y., 2008. Design, synthesis and development of novel camptothecin drugs. Curr. Pharm. 14, 1078-1097. doi: 10.2174/138161208784246180

Liu, T., Hannafon, B., Gill, L., Kelly, W., Benbrook, D., 2007. Flex-Hets differentially induce apoptosis in cancer over normal cells by directly targeting mitochondria. Mol. Cancer Ther. 6, 1814-1822. doi: 10.1158/1535-7163.MCT-06-0279

Liu, X., Situ, A., Kang, Y., Villabroza, K.R., Liao, Y., Chang, C.H., Donahue, T., Nel, A.E., Meng, H., 2016. Irinotecan Delivery by Lipid-Coated Mesoporous Silica Nanoparticles Shows Improved Efficacy and Safety over Liposomes for Pancreatic Cancer. ACS Nano 10, 2702-2715. doi: 10.1021/acsnano.5b07781

Livak, K.J., Schmittgen, T.D., 2001. Analysis of relative gene expression data using real-time quantitative pcr and the 2-ΔΔCT method. Methods 25, 402-408. doi: 10.1006/meth.2001.1262

Mah, L-J., El-Osta, A., Karagiannis, T.C., 2010. γ-H2AX: a sensitive molecular marker of DNA damage and repair. Leukemia 24, 679–686. doi:10.1038/leu.2010.6

Messerer, C.L., Ramsay, E.C., Waterhouse, D., Ng, R., Simms, E.M., Harasym, N., Tardi, P., Mayer, L.D., Marcel B. Bally, M.B., 2004. Liposomal Irinotecan: Formulation Development and Therapeutic Assessment in Murine Xenograft Models of Colorectal Cancer. Clin. Cancer Res. 10, 6638-6649. doi: 10.1158/1078-0432.CCR-04-0221

Michishita, E., Nakabayashi, K., Ogino, H., Suzuki, T., Fujii, M., Ayusawa, D., 1998. DNA topoisomerase inhibitors induce reversible senescence in normal human fibroblasts. Biochem. Biophys. Res. Commun. 253, 667-671. doi: 10.1006/bbrc.1998.9832

Moiseeva, O., Mallette, F.A., Mukhopadhyay, U.K., Moores, A., Ferbeyre, G., 2006. DNA damage signaling and p53-dependent senescence after prolonged β-Interferon stimulation. Mol. Biol. Cell 17, 1583-1592. doi: 10.1091/mbc.E05–09–0858

Morandi, E., Severini, C., Quercioli, D., D'Ario, G., Perdichizzi, S., Capri, M., Farruggia, G., Mascolo, M.G., Horn, W., Vaccari, M., Serra, R., Colacci, A., Silingardi, P., 2008. Gene expression time-series analysis of Camptothecin effects in U87-MG and DBTRG-05 glioblastoma cell lines. Mol. Cancer 7, 1-16. doi: 10.1186/1476-4598-7-66

Neijzen, R., Wong, M.Q., Gill, N., Wang, H., Karim, T., Anantha, M., Strutt, D., Waterhouse, D., Bally, M.B., Tai, I.T., Sylvia S.W. Ng, Yapp, D.T., 2015. Irinophore C™, a lipid nanoparticulate formulation of irinotecan, improves vascular function, increases the delivery of sequentially administered 5-FU in HT-29 tumors, and controls tumor growth in patient derived xenografts of colon cancer. J. Control. Release 199, 72-83. https://doi.org/10.1016/j.jconrel.2014.11.031

Nieves-Neira, W., Pommier, Y., 1999. Apoptotic response to camptothecin and 7-hydroxystaurosporine (UCN-01) in the 8 human breast cancer cell lines of the NCI anticancer drug screen: Multifactorial relationships with topoisomerase I, protein kinase C, Bcl-2, p53, MDM-2 and caspase pathways. Int. J. Cancer 82, 396-404. doi: 10.1002/(SICI)1097-0215(19990730)82:3<396::AID-IJC13>3.0.CO;2-Z

Nishio, K., Inoue, A., 2005. Senescence-associated alterations of cytoskeleton: extraordinary production of vimentin that anchors cytoplasmic p53 in senescent human fibroblasts. Histochem. Cell. Biol. 123, 263-273. doi: 10.1007/s00418-005-0766-5

Pattni, B.S., Chupin, V.V., Torchilin, V.P., 2015. New Developments in Liposomal Drug Delivery. Chem. Rev., 115, 10938–10966. doi: 10.1021/acs.chemrev.5b00046

Peetla, C., Stine, A., Labhasetwar, V., 2009. Biophysical interactions with model lipid membranes: applications in drug discovery and drug delivery, Mol. Pharmaceutics 6 1264-1276. doi:10.1021/mp9000662

Perche, F., Torchilin, V.P., 2013. Recent trends in multifunctional liposomal nanocarriers for enhanced tumor targeting. J. Drug Delivery vol. 2013, Article ID 705265, 32 pages. doi: org/10.1155/2013/705265

Probin, V., Wang, Y., Bai, A., Zhou, D., 2006. Busulfan selectively induces cellular senescence but not apoptosis in WI38 fibroblasts via a p53-independent but extracellular signal-regulated kinase-p38 mitogen-activated protein kinase-dependent mechanism. J. Pharmacol. Exp. Therapeutics 319, 551-560. doi: 10.1124/jpet.106.107771

Przybylo, M., Glogocka, D., Dobrucki, J.W., Fraczkowska, K., Podbielska, H., Kopaczynska, M., Borowik, T., Langner, M., 2016. The cellular internalization of liposome encapsulated protoporphyrin IX by HeLa cells. Eur. J. Pharm. Sci. 85, 39-46. doi: 10.1016/j.ejps.2016.01.028

Ramsay, E., Almajim, J., Anantha, M., Zastre, J., Yan, H., Webb, M., Waterhouse, D., Bally, M., 2008. A novel liposomal irinotecan formulation with significant anti-tumour activity: use of the divalent cation ionophore A23187 and copper-containing liposomes to improve drug retention. Eur. J. Pharm. Biopharm. 68, 607-617. doi: 10.1016/j.ejpb.2007.08.011

Rello, S., Stockert, J.C., Moreno, V., Gámez, A., Pacheco, M., Juarranz, A., Cañete, M., Villanueva, A., 2005. Morphological criteria to distinguish cell death induced by apoptotic and necrotic treatments. Apoptosis 10, 201-208. doi: 10.1007/s10495-005-6075-6

Rello-Varona, S., Herrero-Martín, D., Lopez-Alemany, R., Munoz-Pinedo, C., Tirado, O.M., 2015. "(Not) all (dead) things share the same breath": identification of cell death mechanisms in anticancer therapy. Cancer Res. 75, 913-917. doi: 10.1158/0008-5472.CAN-14-3494

Rodier, F., Campisi, J., 2011. Four faces of cellular senescence. J. Cell. Biol. 192, 547-556. doi: 10.1083/jcb.201009094

Rudolf, E., Rudolf, K., Cervinka, M., 2011. Camptothecin induces p53-dependent and –independent apoptogenic signaling in melanoma cells. Apoptosis 16, 1165-1176. doi: 10.1007/s10495-011-0635-8

Rudolf, E., John, S., Cervinka, M., 2012. Irinotecan induces senescence and apoptosis in colonic cells in vitro. Toxicol. Lett. 214, 1-8. doi: 10.1016/j.toxlet.2012.08.004

Sen, K., Mandal, M., 2013. Second generation liposomal cancer therapeutics: Transition from laboratory to clinic. Int. J. Pharm. 448, 28-43. doi: 10.1016/j.ijpharm.2013.03.006

Shao, R-G., Cao, C-X., Nieves-Neira, W., Dimanche-Boitrel, M-T., Solary, E., Pommier, Y., 2001. Activation of the Fas pathway independently of Fas ligand during apoptosis induced by camptothecin in p53 mutant human colon carcinoma cells. Oncogene 20, 1852-1859. doi: 10.1038/sj.onc.1204264

Sharma, A., Singh, K., Almasan, A., 2012. Histone H2AX phosphorylation: A marker for DNA damage, in Methods Lotte, Bjergbæk., (Ed.), Molecular Biology: DNA Repair Protocols. Springer Science+Business Media, New York, vol. 920, pp. 613–626. doi: 10.1007/978-1-61779-998-3_40, ©

Sinha, R., Kim, G.J., Nie, S., Shin, D.M., 2006. Nanotechnology in cancer therapeutics: bioconjugated nanoparticles for drug delivery. Mol. Cancer Ther. 5, 1909-1917. doi: 10.1158/1535-7163.MCT-06-0141

Tamura, N., Hirano, K., Kishino, K., Hashimoto, K., Amano, O., Shimada, J., Sakagami, H., 2012. Analysis of type of cell death induced by topoisomerase inhibitor SN-38 in human oral squamous cell carcinoma cell lines. Anticancer Res. 32, 4823-4832.

Teicher, B.A., 2008. Next generation topoisomerase I inhibitors: Rationale and biomarker strategies. Biochem. Pharmacol. 75, 1262-1271. doi: 10.1016/j.bcp.2007.10.016

Torchilin, V.P., 2005. Recent advances with liposomes as pharmaceutical carriers. Nature Reviews Drug Discovery 4, 145–160. doi:10.1038/nrd1632

Vanhoefer, U., Harstrick, A., Achterrath, W., Cao, S., Seeber, S., Rustum, Y.M., 2001. Irinotecan in the Treatment of Colorectal Cancer: Clinical Overview. J. Clin. Oncol. 19, 1501-1518.

Wei, H., Song, J., Li, H., Li, Y., Zhu, S., Zhou, X., Zhanga, X., Yanga, L., 2013. Active loading liposomal irinotecan hydrochloride: Preparation, in vitro and in vivo evaluation. Asian J. Pharm. Sci. 8, 303-311. doi: 10.1016/j.ajps.2013.10.006

Wolterbeek, H.T., van deer Meer, A.J.G.M., 2005. Optimization, application, and interpretation of lactate dehydrogenase measurements in microwell determination of cell number and toxicity. Assay Drug Dev. Technol. 3, 675-682. doi: 10.1089/adt.2005.3.675

Wu, M.H., Yan, B., Humerickhouse, R., Dolan, M.E., 2002. Irinotecan activation by human carboxylesterases in colorectal adenocarcinoma cells. Clin. Cancer Res. 8, 2696-2700.

Legends to Figures

Fig 1. Uptake and mechanisms of cell entry of CPT-11sol and CPT-11lip into Hs68 and HeLa cells. A) The graphs show the quantitative analysis of the internalization of CPT-11 in Hs68 (a) and HeLa (b) cells carried out by flow cytometry. Cells were incubated with 100 μM CPT-11lip (light symbols) or 100 μM CPT-11sol (dark

symbols) for different periods of time, at 37°C. Emission fluorescence at 450 nm was determined after excitation at 405 nm. Data are the means ± SD from three different experiments. Significance was assessed using a Student's paired t-test, being P<0.0014 and P<0,018 for Hs68 and HeLa cells, respectively. B) Incubations with CPT-11lip and CPT-11sol for 3 h at 4 °C visualized by fluorescence (UV excitation) and merged images with phase-contrast microscopy. (a, b) Hs68 cells incubated with CPT-11sol. (c, d) HeLa cells incubated with CPT-11sol. (a', b') Hs68 cells incubated with CPT-11lip . (c', d') HeLa cells incubated with CPT-11lip. Scale bar: 10 µm.

Fig 2. Assessment of cell survival at different times (0, 24 and 48 h) after CPT-11 removal. (A, B) Surviving fraction of Hs68 and HeLa cells incubated 48 h with 100 µM CPT-11lip or CPT-11sol evaluated by MTT assay, respectively. (C, D): Surviving fraction of Hs68 and HeLa cells measured by Trypan blue assay, respectively. Data correspond to mean values ± standard deviation from at least eight different experiments for MTT assay and four different experiments for Trypan blue assay. P values <0.05 (*), 0.005 (**), 0.001 (***), and 0.0001(****) were considered as statistical significant.

Fig 3. Analysis of CTP-11lip localization. A) (a,e) Confocal microscopy fluorescence images of LysoTracker® Green under blue exciting light, merged with differential interference contrast (DIC) microscopy of control Hs68 and HeLa cells, respectively. B) Cells were treated with CPT-11lip (100 µM) for 24 h and counterstained with LysoTracker® Red DND-99, before being observed by DIC and confocal microscopy. (b-d) Hs68 cells show blue fluorescent spots in the cytoplasm that almost completely co-localize with LysoTracker® Red. (f-h) HeLa cells show a similar subcellular distribution pattern. Scale bars: 10 µm.

Fig 4. Morphological changes after treatment. Cell morphology visualized by toluidine blue staining immediately, 24 and 48 h after CPT-11lip treatment. A) Analysis of Hs68 cells. (a-c) Untreated (control) Hs68 cells. (a'-c') Treated Hs68 cells: CPT-11lip did not cause loss of cell adhesion or cell morphology changes in Hs68 cells at different times after incubation. B) Analysis of HeLa cells. (a-c) Control HeLa cells. (a'-c') Treated HeLa cells: the vast majority of HeLa cells were detached from plastic after CPT-11lip incubation. Note that the few remaining adherent cells changed their shape and size.

Fig 5. Identification of apoptotic HeLa cell death induced by 100 µM CPT-11lip. A) LDH assay results. Statistical analysis showed that there was no significant difference between the control (C) and CPT-11lip treated (T) cells. B) Detached HeLa cells after 48 h of incubation with liposomal CPT-11 stained with H-33258. (a) Low magnification. (b, c) Images taken at a higher magnification. Scale bars 10 µm. C) Confocal fluorescence merged images of HeLa cells visualized by Bax immunofluorescence (green) and H-33258 counterstaining of nuclei

(blue). (a) Control cells with diffuse Bax signal in the cytosol. (b) Images of translocation of Bax protein from the cytosol into mitochondria of HeLa cells. Scale bars: 10 μm. (c) Apoptotic cell at higher magnification.

Fig 6. Cell cycle analysis and senescence-associated β-galactosidase assay. (A, B) Effects of CPT-11lip on cell cycle phase distribution on Hs68 and HeLa cells, respectively. Results were obtained from two independent experiments. For each experiment, a minimum of 20 000 events were analyzed. (C) Cellular senescence-associated β-galactosidase activities at 0 (immediately), 2 and 5 days after incubation. Percentages of senescent cells referred to the total amount of cells on the plate. Results are the mean of three different experiments ± SD. (D) Images correspond to a representative assay. Scale bars: 10 μm.

Fig 7. Time-dependent effects of incubation with CPT-11lip on mRNA expression levels of p53, Bax and Bcl-2 by real-time PCR assay. A) RT-PCR in Hs68 cells. B) RT-PCR in HeLa cells. GAPDH mRNA was used as an internal control. Results are represented as the log10 of the relative quantity normalized to control cells. Data are means ± SD from at least three different experiments. Significance was assessed using Student's t test: *$P<0.05$, and **$P<0.005$.

Fig 8. F-actin and vinculin in Hs68 and HeLa cells after incubation with CPT-11lip. A) Cytoskeleton confocal images of Hs68 cells observed in control (a-d) and immediately, 24 or 48 h (e-p) after drug removal, respectively. B) The same analysis was performed in HeLa cells. F-actin structures are shown in red (stained with phalloidin-TRITC), green corresponds to immunolabelling of vinculin, the blue signal refers to chromatin (stained with H-33258), and last column to overlay images. The cells shown in each panel are representative of predominant morphologies observed in four separate experiments. Scale bars: 20 μm.

Fig9. Immunofluorescent analysis of γ-H2AX. A) Representative images of Hs68 cells immunostaining to H2AX γ-phosphorylated histone (green), counterstained with H-33258 (blue), merged images and overlay of fluorescence and phase-contrast microscopy (PC) at three different incubation times with CPT11-lip. (a-d) Control Hs68 cells. (e-h), (i-l), (m-p) Cells after 3, 6 and 24 h of incubation, respectively. B) Representative images of HeLa cells under the same experimental conditions. Scale bars: 10 μm.